HHS Public Access

Author manuscript

Nat Struct Mol Biol. Author manuscript; available in PMC 2017 June 12.

Published in final edited form as:

Nat Struct Mol Biol. 2016 November ; 23(11): 974–981. doi:10.1038/nsmb.3298.

Substrate-Translocating Loops Regulate the Mechanochemical Coupling and Power Production in a AAA+ Protease

Piere Rodriguez-Aliaga[1,2,3], **Luis Ramirez**[1,3], **Frank Kim**[1], **Carlos Bustamante**[1,2,3,4,5,6,7,*], and **Andreas Martin**[2,3,4,6,*]

[1]Jason L. Choy Laboratory of Single-Molecule Biophysics, University of California at Berkeley, Berkeley, California, USA

[2]Biophysics Graduate Group, University of California at Berkeley, Berkeley, California, USA

[3]Institute for Quantitative Biosciences-QB3, University of California at Berkeley, Berkeley, California, USA

[4]Department of Molecular & Cell Biology, University of California at Berkeley, Berkeley, California, USA

[5]Department of Chemistry and Department of Physics, University of California at Berkeley, Berkeley, California, USA

[6]Howard Hughes Medical Institute, University of California at Berkeley, Berkeley, California, USA

[7]Kavli Energy Nanosciences Institute, University of California at Berkeley, Berkeley, California, USA

Abstract

ATP-dependent proteases of the AAA+ family, including *Escherichia coli* ClpXP and the eukaryotic proteasome, contribute to maintenance of cellular proteostasis. ClpXP unfolds and translocates its substrates into an internal degradation chamber using cycles of alternating dwell and burst phases. The ClpX motor performs chemical transformations during the dwell and translocates the substrate in 1-4 nm increments during the burst, but what processes occur during these phases remains unknown. Here we characterize the complete mechanochemical cycle of ClpXP, showing that ADP release and ATP binding happen non-sequentially during the dwell, while ATP hydrolysis and phosphate release occur during the burst. The highly-conserved translocating loops within the ClpX pore are evolutionarily optimized to maximize motor power generation, the coupling between chemical and mechanical tasks, and the efficiency of protein processing. Conformational resetting of these loops between consecutive bursts seems to determine ADP release from individual ATPase subunits and the overall duration of the motor's cycle.

Correspondence should be addressed to C.B. (carlosb@berkeley.edu) or A.M. (a.martin@berkeley.edu).

Supplemental Information: Supplemental Information includes six figures and Online Methods.

Author Contributions: P.R.A. designed, performed and analyzed most of the experiments with input from C.B. and A.M. L.R. and F.K. contributed to most of the experiments and assisted with cloning, protein purification, and part of data acquisition with optical tweezers. P.R.A., C.B., and A.M. wrote the manuscript.

Competing Financial Interests: The authors declare no competing financial interests.

Like most AAA+ proteases, the bacterial ClpXP consists of two major components (Fig. 1a): i) the AAA+ ATPase ClpX, a homo-hexameric ring with an axial processing pore, and ii) the barrel-shaped ClpP peptidase, which contains proteolytic active sites sequestered in an internal chamber. One of the signals that target protein substrates for degradation by *E. coli* ClpXP is the ssrA-tag, a 11-amino acid sequence that is appended to the C-terminus of incompletely translated proteins at the ribosome[1]. SsrA-mediated degradation comprises three ATP-dependent steps[2–4]: i) recognition and engagement of the protein through ssrA-tag binding to the ClpX pore, ii) force-induced unfolding, which results from the mechanical pulling and translocation of the ssrA-tagged protein into the narrow central pore, and iii) translocation of the unfolded polypeptide into the associated ClpP peptidase for degradation (Fig. 1a). Polypeptide translocation is therefore the fundamental mechanical activity of ClpXP. A translocating loop with a highly-conserved glycine-tyrosine-valine-glycine (GYVG) motif protrudes from every ClpX subunit into the central pore (Fig. 1b). These GYVG loops (also referred to as pore-1 loops) make direct contact with the substrate and transduce the ATP-hydrolysis-driven motions of the motor subunits to propel the substrate by individual power strokes[5–7].

Recently, single-molecule manipulation studies[8–10] unveiled important aspects of ClpXP's operation that were not accessible by traditional bulk or structural studies. Using optical tweezers, it was established that substrate translocation by ClpXP is composed of two phases: a “dwell” or stationary phase, where ClpXP does not move its substrate, and a “burst” phase, wherein ClpXP translocates the substrate in increments of 1, 2, 3 or 4 nm, resulting from the near-simultaneous ATP-driven conformational changes of 1, 2, 3, or 4 ClpX subunits, respectively[9,10] (Fig. 2a). Translocation is occasionally interrupted by pauses longer than 1s, during which the motor temporally accesses a state off the main translocation pathway[9]. The off-pathway character of these pauses is indicated by an inverse correlation between the translocation velocity and the pause density, which is consistent with a kinetic competition between moving the substrate and entering a pause[9]. Interestingly, while the ClpXP burst size is variable, the mean dwell duration between individual bursts is constant[8]. Thus, the operation of ClpXP deviates significantly from those of canonical ring-shaped molecular machines such as the ϕ29 DNA-packaging motor[11,12] and the F1-ATPase rotary motor[13], which display constant bursts followed by dwells of variable length. Yet, the underlying molecular processes behind this distinct ClpXP operation remain unknown.

Here, we set out to dissect the mechanochemical mechanisms of ClpXP. We show when each transition of the ATP-hydrolysis cycle occurs within the mechanochemical dwell/burst cycle of ClpXP and identify the molecular processes that govern each phase. Moreover, we demonstrate that the chemical identity and dynamics of the GYVG loops regulate the mechanochemical coupling efficiency and power production of ClpXP. These results highlight how evolution has optimized AAA+ proteases for efficient protein processing. Given their strong conservation and high homology, it is likely that other AAA+ protein translocases work by similar mechanisms as those identified here for ClpXP.

Results

ATP hydrolysis occurs in the burst phase

We used a dual-trap optical-tweezers setup, similar to the one previously described[9], to track in real-time a single ClpXP molecule as it mechanically unfolds and translocates an ssrA-tagged protein in the presence of ATP (Fig. 1c). Our model substrate contains a green fluorescent protein (GFP) moiety and four C-terminally fused titin I27 domains that are permanently unfolded by carboxymethylation (Ti^{CM}), followed by an ssrA tag. ClpXP and its protein substrate were individually immobilized on the surface of two micron-sized polystyrene beads that were held in separate optical traps. After engaging the substrate, ClpXP immediately proceeds to translocate the Ti^{CM} moieties, decreasing the distance between the beads held in the fixed traps (passive mode; Fig. 1c). GFP unfolding events appear as sudden extension gains, which are followed by a steady decrease in extension due to the processive translocation of the unfolded substrate into ClpXP. Periods with no extension change for longer than ~1s indicate motor pauses off the main translocation pathway.

To characterize the mechanochemical cycle, we inhibited hydrolysis in different numbers of ClpX subunits by using various concentrations of ATPγS, an ATP analog hydrolyzed ~ 90 times slower than ATP[8], and analyzed its effects on the dwell and burst phases. We reported previously that the addition of ATPγS in the presence of ATP induces translocation pauses, whose duration and frequency increase with the ATPγS concentration[8]. It is noteworthy that those pauses occur with equal probability over the entire length of the substrate polypeptide and are not significantly affected by sequence features.

First, we determined how many subunits needed to bind ATPγS to induce a translocation pause. Because only four of the six ATPase sites in ClpX can bind nucleotide in every cycle[14,15], the probability of binding i or more ATPγS molecules to the motor is given by $\sum_i^4 \frac{4!}{i!(4-i)!} p^i q^{4-i}$, where p is the fraction of all nucleotide-bound subunits that is occupied with ATPγS at particular ATPγS and ATP concentrations, and $q = 1 - p$ (Online Methods). Because the nucleotide off-rate after initial binding appears to be low and tight-binding before hydrolysis is the first irreversible step in the ATPase cycle of ClpX[8], bound ATPγS cannot be readily exchanged for ATP, and it is therefore possible to directly correlate ATPγS occupancy of the motor with the probability of entering a pause. This probability is 50 % at [ATPγS] = 200μM and [ATP] = 500μM[8]. Here we calculate that under the same conditions the probability of binding two or more ATPγS molecules to ClpX is also ~ 50 % (Fig. 2b). Thus, binding of two or more subunits to ATPγS temporarily stalls the motor.

Next, we analyzed the effect of ATPγS on the dwell duration and the burst size during pause-free translocation. While the mean dwell duration remained unchanged, the mean burst size decreased with increasing [ATPγS] (Fig. 2c), as indicated by the absence of 4-nm bursts and the increase of 1-nm bursts (Supplemental Fig. 1a). Since under our experimental conditions the probability of one or more ATPγS molecules binding to ClpXP is ~ 90% (Fig. 2b), the absence of 4-nm bursts is likely due to the presence of at least one ATPγS-bound subunit in the hexamer during every cycle. Thus, although binding of a single ATPγS cannot induce a pause, it hinders the binding of an ATP molecule to the motor and thereby reduces the burst size. Based on these observations we can conclude that the burst size reflects the number of ATP-loaded ClpX subunits during a particular cycle.

Having established that binding of two or more ATPγS molecules to the ClpX motor causes an ATPγS-induced pause, we sought to utilize these pauses for determining where in the dwell/burst cycle ATP hydrolysis occurs. We observed that ATPγS-induced pauses are both preceded and followed by bursts of only 1 or 2 nm, with 3 and 4-nm bursts being notably absent (Fig. 2d). This behavior is consistent with a model in which one or two subunits hydrolyze ATP and translocate the substrate, before the ATPγS-bound subunits attempt to hydrolyze and induce a pause that terminates the ongoing burst. The burst subsequent to the ATPγS-induced pause would also be truncated, because the ATPγS-bound subunits were not available for ATP binding in that following cycle. ATP hydrolysis thus appears to occur during the burst phase, which is further supported by our finding that the addition of ATPγS has no effect on the dwell duration (Fig. 2c). Moreover, the existence of smaller bursts before an ATPγS-induced pause suggests that hydrolysis events are interlaced with the power-stroke-generating release of phosphate, i.e. successful ATP hydrolysis in a ClpX subunit is immediately followed by phosphate release, conformational changes, and substrate translocation by a 1-nm increment, before hydrolysis in a neighboring subunit is initiated.

It has been proposed that nucleotide binding induces asymmetry in the ClpX hexamer, with two high-affinity, two low-affinity, and two unloadable sites, and that subunits may convert between these states through conformational switching after each ATPase cycle[14,16]. This model for the switching of affinity states among subunits could explain how an ATPγS-induced pause can be both preceded and followed by truncated bursts. Assuming that high-affinity sites hydrolyze first during an ATPase cycle, a 1 or 2-nm burst before an ATPγS-induced pause may originate from one or two ATPs binding and hydrolyzing in high-affinity subunits, while the low-affinity sites are occupied with ATPγS. During the subsequent ATPγS-induced pause, the high-affinity sites would release their ADP, and the ATPγS-bound subunits may switch from the low to the high-affinity state, as they are the first subunits to be occupied with nucleotide in the new ATPase cycle. The empty low-affinity subunits could then fill with one or two ATPs, but would not be able to hydrolyze until at least one of the high-affinity subunits releases its ATPγS (Supplemental Fig. 1b). Based on our previous comparison between the duration of ATPγS-induced pauses and the time constant for ATPγS hydrolysis[8], we can conclude that ATPγS dissociation, not hydrolysis, likely determines the end of the ATPγS-induced pause and the onset of hydrolysis in the ATP-bound subunits to generate the next truncated burst. In case ATPγS initially binds to both high-affinity subunits, ClpX would enter an ATPγS-induced pause right away and continue translocation afterwards with a truncated burst. However, this scenario is less likely due to the at least two-fold excess of ATP over ATPγS in our experiments.

ADP release and ATP binding occur in the dwell phase

To reveal when ADP is released within the dwell/burst cycle, we lowered the rate of ADP dissociation through the addition of orthovanadate (VO_4^{3-}), a Pi analog whose binding temporally traps ADP in the nucleotide-binding pocket[17,18]. At saturating [ATP], the addition of VO_4^{3-} significantly reduced the pause-free translocation velocity of ClpXP (Fig. 3a) as well as its bulk ATPase rate (Supplemental Fig. 2a), but had no effect on the frequency or duration of off-pathway pauses (Supplemental Fig. 2b). As shown in Fig. 3b and Supplemental Fig. 2c, the burst-size distribution remained unchanged, whereas the mean dwell duration significantly increased with increasing [VO_4^{3-}], indicating that ADP release occurs during the dwell.

On the other hand, ATP binding must occur after the release of ADP, but before ATP hydrolysis (Fig. 2a). Because ADP is a competitive inhibitor of ClpXP[8,14], ATP binding can occur as soon as ADP was released from a particular subunit and does not require ADP release from all other subunits in the hexamer. Scenarios where all ADP release and ATP-binding events occur temporally segregated can therefore be ruled out (Supplemental Fig. 3a), and we can conclude that both ADP release and ATP binding happen during the dwell (Fig. 3d). Interestingly, we observed a Hill coefficient for ATP binding and hydrolysis of ~1.6 (Fig. 3c, Supplemental Fig. 3b), indicating that on average more than one ATPase site in the ClpX hexamer is available for ATP binding. Therefore, albeit interlaced, ADP release and ATP binding are not strictly sequential for successive ClpX subunits. This scenario is in contrast to the mechanism observed for the F1-ATPase rotary motor[13] or the ϕ29 DNA packaging motor[11,19], which bind ATP around the ring strictly interlaced with ADP release and therefore display a Hill coefficient of 1.

ADP release is the rate-limiting chemical transition of the dwell

ADP release and ATP binding both occur during the dwell phase, but which one is the rate-limiting step of this phase? To answer this question, we calculated the value of n_{min} as a lower bound for the number of rate-limiting events during the dwell[12,19,20]. n_{min} is given by the ratio of the squared mean dwell duration over its variance, $n_{min} = <\tau>^2/(<\tau^2> - <\tau>^2)$. For ClpXP we previously reported a value of $n_{\mathrm{min}} \sim 2$, indicating that two or more rate-limiting events govern the duration of the dwell, and that those events are likely not associated with ATP binding, since the dwell duration is independent of [ATP] in the range between K_M and saturation[8]. Thus, ADP release is probably the rate-determining step of the dwell. To test this hypothesis we analyzed whether n_{min} remains unchanged when ADP release is slowed by the presence of VO_4^{3-}. Despite a ~40% increase in dwell duration, increasing [VO_4^{3-}] did not affect n_{min} (Fig. 3e), consistent with ADP release being rate limiting for dwell duration at saturating [ATP].

GYVG loops determine the mechanochemical coupling efficiency

After focusing solely on the chemical cycle, we sought to investigate its coupling to the mechanical cycle by perturbing the translocating GYVG loops. These loops are highly-conserved among most prokaryotic and eukaryotic AAA+ protein translocases (Fig. 1b) and are thought to contact and transmit mechanical force to the substrate[6,7,21]. By introducing the Y153A or V154F mutation, we decreased or increased the loop size, respectively (Fig. 4a), and analyzed the effects on the dwell/burst cycle as well as the role of the GYVG loop in the mechanochemistry of ClpX. The use of single-chain constructs with six covalently linked ClpX subunits[22] allowed us to create pseudo-hexamers with different numbers and spatial arrangements of GYVG-mutated subunits.

We first characterized how the increase or decrease of bulkiness inside the ClpX pore affected the translocation velocity at saturating [ATP] (Fig. 4b, c). The pause-free velocity of Y153A mutants increased with the number of mutated subunits, whereas it decreased with increasing number of V154F subunits. Thus, the motor's pause-free velocity is inversely related to the bulkiness of the loops inside the ClpX pore, suggesting that the movement of these loops is affected by their steric hindrance. Importantly, GYVG mutations do not increase the mean frequency or duration of pauses during translocation (Supplemental Fig. 4a), except for a specific region in the protein substrate that surrounds the cyclic chromophore of the GFP moiety (Supplemental Fig. 6). The duration and frequency of this sequence-induced pause is significantly higher for V154F mutants compared to WT ClpXP, while Y153A mutants pause in this specific region as infrequently as throughout the rest of the substrate (Fig. 5c). This analysis reinforces the idea that bulkiness inside the ClpX pore —originating from the motor loops and the translocating substrate— affects the movement of the translocating loops.

Next, we determined the bulk ATPase rate of the GYVG loop mutants as they translocate the permanently unfolded protein substrate Ti^{CM}-ssrA, present at 500 μM to ensure saturation (Fig. 4c; Supplemental Fig. 3b). Compared to WT, the ATPase rate of Y153A mutants is increased by 100 % - 200 %, a trend that is consistent with a recent independent study of these mutants[23]. Interestingly, for V154F mutants we observe a modest increase of only ~ 40 %. Thus, GYVG mutations affect both, the mechanical and chemical cycles of the motor.

Are all additional ATP-hydrolysis events observed in the ClpX mutants coupled to translocation? Dividing the pause-free velocity (nm/s) by the ATP-turnover value (ATP/s) for each GYVG mutant yields the coupling coefficient (ε), which is a measure for the fraction of ATP-hydrolysis cycles that result in successful substrate translocation (Fig. 4d). Consistent with previous reports[9,10,21], we find for WT that $\varepsilon \sim 1$ nm/ATP, i.e. every ATP hydrolyzed results in translocation of the substrate by 1 nm. In contrast, we find $\varepsilon \sim 0.5$ for the Y153A mutants, and $\varepsilon \sim 0.65$ for the V154F mutants. A scenario, where every ATP hydrolysis results in translocation, but with a reduced step size of 0.5 nm or 0.65 nm, can be ruled out based on our finding that GYVG mutations do not affect the burst size of the motor (Fig. 5a, Supplemental Fig. 5a). Alternatively, an increased ATP consumption could theoretically be caused by defects in initial substrate engagement, but only if the basal ATPase rate—i.e., the rate in the absence of protein substrate—is higher than the ATPase rate during substrate processing. This model can also be dismissed, as the basal ATPase rates of WT and the GYVG mutants are actually 4-6 times lower than the rates during protein translocation (Supplemental Fig. 4b). Interestingly, a recent bulk study[23] reported that Y153A mutants have a mechanochemical coupling twice as efficient as WT ($\varepsilon \sim 2$), which is contrary to our results here and may have arisen from non-saturating substrate concentrations used in those ATPase measurements. Our data suggests that a significant fraction of ATP-hydrolysis events in GYVG mutants actually fail to propel the substrate due to an altered interaction between the loops and the polypeptide, reducing the mechanochemical coupling of the motor.

To evaluate whether GYVG loop mutations affect the grip of the motor, i.e. the strength of contacts with the substrate, we investigated how the translocation velocity of GYVG mutants is affected by increasing external force (F_{ext}) that opposes the force exerted by the motor (F_M) (Fig. 4e). At the stall force, F_{ext} equals the maximum force exerted by the motor, and the translocation velocity reaches zero. By fitting the force dependence of the pause-free velocity to a single-barrier Boltzmann equation[24], we obtained $F_{1/2}$, the external force at which the translocation velocity drops to half its maximum value (Online Methods).

Not knowing the complete force-velocity curve for ClpXP, we cannot simply assume that $F_{1/2}$ equals $F_M / 2$, but the ratio $F_{1/2} / F_M$ is expected to be identical for different ClpX variants, as F_{ext} has to counterbalance F_M to a similar extent to reach half-maximal translocation velocity for those motors. Thus, we propose that observed differences in $F_{1/2}$ can be related to corresponding changes in F_M, or motor grip, caused by mutations in the GYVG loops. For WT we can extrapolate $F_{1/2} = 20.5 \pm 1.3$ pN, while a Y153A mutation in the 1st and 4th subunits (YA14) showed $F_{1/2} = 15.1 \pm 1.1$ pN, indicating that translocation in Y153A mutants is significantly more sensitive to force compared to WT. Further extrapolation based on the single-barrier Boltzmann model indicates that WT ClpX would drop to 5 % of its maximum translocation velocity at ~35 pN (Fig. 4e), which is in good agreement with previous predictions of its stall force[10], whereas the YA14 mutant would reach that 5 % velocity already at ~25 pN. In contrast, the variant with V154F mutation in the 1st and 4th subunits (VF14) was insensitive to force up to 13 pN, implying a F1/2 and stall force larger than for WT. Thus, Y153A mutations seem to reduce the grip on the substrate, which agrees with the results from a recent single-molecule study on Y153A mutants[29], while V154F mutations appear to improve it. Despite this better grip, V154F mutants display a fraction of futile translocation attempts, as indicated by their lower coupling coefficient discussed above. One possible explanation is that the V154F mutation interferes somewhat with the pore integrity, the arrangement or movement of pore loops, or their interaction with substrate, thus leading to some futile translocation attempts.

In summary, GYVG-loop residues appear to have been selected for optimal coupling between the chemical and mechanical cycles of the motor by providing enough grip on the substrate, without increasing the steric hindrance inside the ClpX pore (See Discussion).

GYVG mutations alter the duration of the dwell

Surprisingly, we found that the burst size remains invariable for all Y153A and V154F mutants compared to WT (Fig. 5a). This result indicates that the intersubunit coordination of ATP-hydrolysis and Pi-release events during the burst occurs by a GYVG-loop-independent mechanism, which agrees with the proposed model that ATP-hydrolysis-induced conformational changes in one subunit are communicated to neighboring subunits through a topologically constrained set of rigid-body units and hinges that conform the ClpX ring[15,16,25]. Interestingly, ClpX mutants that lack the tyrosine in three of the six GYVG loops (e.g. YA156 and YA146) still produced 4-nm bursts (Supplemental Fig. 5a), which is consistent with a recent independent single-molecule study of these mutants[29]. This behavior can be rationalized if substrates are propelled primarily through contacts with the GYVG loop's backbone, while the tyrosine side chains provide additional contacts and thus a stronger grip on the substrate. Alternatively, these findings would also be consistent with a recently proposed model in which several GYVG loops grip the substrate simultaneously and work synergistically for translocation[23,29]. ATP-hydrolysis and Pi release in pore-loop defective subunits may thus still drive substrate translocation through coupling with neighboring, intact subunits, albeit at the expense of grip and the maximum force that can be applied for unfolding.

In contrast to the unchanged burst-size distribution, the mean dwell duration compared to WT is significantly shorter for Y153A mutants and prolonged for V154F mutants, with the observed changes being proportional to the number of mutant subunits in the ring (Fig. 5a). Importantly, these changes in dwell duration solely account for all the measured differences in pause-free velocities of GYVG mutants (Supplemental Fig. 4c).

Our results can be best rationalized if the conformational changes in the GYVG loops during the dwell are coupled to the rate-limiting chemical transition that governs the dwell duration, i.e. the release of ADP, and that GYVG mutations may therefore alter the rate of ADP release. Consistent with this hypothesis, we observed that GYVG mutations affect the ATPase Vmax (Fig. 5b), which depends on all microscopic rate constants except ATP binding[19,26,27] (Fig. 2a), but have no effect on Vmax/K_M, which is determined only by the microscopic rate constant of initial ATP docking and tight-binding[19,26,27]. Thus, GYVG mutations should affect one or several of the chemical transitions after the irreversible tight-binding of ATP, i.e. ATP hydrolysis, release of Pi, or release of ADP. Out of these transitions only ADP release occurs in the dwell, and we therefore conclude that GYVG mutations likely affect ADP release from ClpX subunits. Consistent with this conclusion, the mean dwell duration of a variant with two mutated tyrosines (YA14) did not change when [ATP] was reduced to near K_M (Supplemental Fig. 5b). Limiting [ATP] only decreased the mean burst size and eliminated 4-nm bursts for this mutant, very similar to the effects on WT ClpX[8].

Since ADP release occurs after the power stroke and before binding of a new ATP molecule, the GYVG-loop movements linked to this ADP release likely correspond to the loops resetting back into a position that allows them to tightly grip the substrate upon ATP binding and to execute the next power stroke after hydrolysis and Pi release (Figure 5d). Our results thus uncover a previously unknown mechanism for AAA+ motors by which both the chemical and mechanical cycles of the ATPase subunits are set anew through a single coupled conformational change that is affected by the bulkiness of the translocating pore-loop residues. Bulkier pore-loop residues increase the grip on the substrate polypeptide, but at the expense of additional steric hindrance that slows the mechanical and chemical resetting of the ATPase and leads to lengthening of the dwell time. In contrast, smaller pore-loop residues accelerate the mechanochemical resetting of the motor and thus shorten the dwell, but reduce the grip strength.

GFP unfolding depends on the power produced by the motor

Protein unfolding represents a higher mechanical barrier for the motor than translocation of an unstructured polypeptide. To test whether the side chains of the GYVG loops have been optimized to enable robust protein unfolding, we analyzed the effects of GYVG mutations on the ability of ClpXP to unfold the GFP moiety in our model substrate. For each GYVG mutant we calculated the GFP-unfolding probability as the number of traces displaying a GFP-unfolding event divided by the total number of traces (Fig. 6a). We found that a Y153A or V154F mutation in a single ClpX subunit lowers the GFP-unfolding probability compared to WT by 50 %, which further decreases with increasing number of mutant subunits in the ring (Fig. 6b). The side chains of the GYVG loops are thus critical for the motor's ability to mechanically unfold GFP.

We previously proposed that GFP unfolding by WT ClpXP requires the near-simultaneous firing of four subunits[8], i.e. 4 nm bursts, which occur only at saturating [ATP]. Contrary to this model, however, we show here that GYVG mutants are strongly compromised in their ability to unfold GFP, even though they display the same frequency of 4-nm bursts as WT (Supplemental Fig. 5a). It was recently proposed that GFP unfolding by ClpXP depends on the coordinated and simultaneous gripping of a high enough number of ClpX subunits[23,29]. Yet, we found that V154F mutants, which grip the substrate with higher strength than WT (Fig. 4e), are as inefficient in unfolding GFP as the Y153A mutants that display reduced grip strength. Thus, the burst size of the motor or its grip strength independently cannot explain the mechanism of GFP unfolding by ClpXP.

As shown in Fig. 6b, the GFP unfolding probability reaches a maximum at the intermediate GYVG-loop residue size of WT ClpX. This maximum likely originates from the product of two contributions: one that increases with pore-loop residue size and another one that decreases accordingly. Because the force (F_M) that ClpXP applies to the substrate and its translocation velocity (v) increases and decreases, respectively, with the pore-loop residue size (Fig. 4c-4e), their product—i.e. the amount of power (P) generated by the motor—should make a maximum at a certain pore-loop residue size. We therefore propose that the unfolding ability of ClpXP depends on the motor's generated power (P). Specifically, ClpXP's power output is the product of its force (F_M) applied to a substrate –which equals the external opposing force F_{ext}– and its translocation velocity at that particular force, $v(F_{ext})$. Thus, with $P = F_M \bullet v(Fext)$, the power output depends on the external opposing force and approaches zero when F_{ext} is either zero or equals the maximum force of the motor.

For WT ClpXP and its mutants we calculated the power output at $F_{1/2}$, which is close to half the maximum force produced by the motors (Fig.4e). The product of the motor's force and velocity at $F_{1/2}$ is close to the maximum power output. Under these conditions, WT ClpX is able to produce $P_{WT} = 90.2 \pm 3.1$ $pN\,nm\,s^{-1}$, whereas for YA14 this value is only $P_{YA14} = 80 \pm 2.9$ $pN\,nm\,s^{-1}$ (Online Methods). The stronger grip of the VF14 mutant made its $F_{1/2}$ experimentally inaccessible (expected to be larger than WT) and thus prevented us from calculating P_{VF14}.

Our analysis suggests that Y153A mutants fail 2-3 times more frequently than WT in unfolding GFP, because their weaker grip on the substrate reduces the work produced to overcome the mechanical unfolding barrier, even at the maximum burst size of 4 nm. V154F mutants, on the other hand, grip the substrate with a higher strength and produce more work than WT, but still unfold GFP with significantly reduced efficiency, likely due to their lower pulling frequency. This lower frequency results in reduced motor power and may allow GFP-unfolding intermediates to refold in between pulling events. We previously observed that GFP unraveling from the C terminus begins with the extraction of β-strand 11 (β11), which has a strong tendency of refolding within ~ 230 ms[8]. To completely unfold GFP, ClpXP must therefore produce enough work to overcome the initial unfolding barrier, but then also translocate β11 faster than its refolding time. V154F mutants may thus fail to unfold GFP because their dwell duration (> 320ms) is significantly larger than the refolding time of β11 (Fig. 6c). Consistent with this hypothesis, we observed β11 extraction and refolding events with much higher frequency in traces for V154F mutants than for WT or Y153A mutants (Fig. 6d).

Discussion

Our power-based model also explains why ClpA, a *double*-ring AAA+ protease machine, is a better unfoldase than ClpX. A recent single-molecule study[28] showed that ClpA grips the substrate with a very similar strength as the ClpX V154F mutants shown here, suggesting that ClpAP produces more work per translocation burst than WT ClpXP. Since the pulling rate of ClpAP and ClpXP are similar[28], our model predicts that ClpAP generates more *power* than ClpXP, potentially due to additional substrate contacts conferred by the extra AAA+ ring or differences in the pore loops.

Our analysis of motor power reconciles in a single parameter all the different—and sometimes antagonistic—models currently available for the unfolding efficiency of ClpX and related AAA+ protein translocases. This parameter, the product of generated force and translocation velocity, appears to be optimal for the WT GYVG-loop sequence, suggesting that evolution has selected the bulkiness of the loop residues to maximize the power generated by the motor. An optimal level of bulkiness inside the crowded ClpX pore may ensure an ideal compromise between the grip of the motor on the substrate and its pulling frequency (Fig. 6e).

In summary, our results constitute the first comprehensive mechanochemical characterization of an AAA+ protein translocase. We provide a detailed picture of how the chemical transitions in the ClpX ATPase cycle are coupled to the dwell and burst phases of the motor, and show that the GYVG pore loops of ClpX play crucial roles in the mechanochemical coupling, power production, and conformational resetting after a power stroke. Given their high homology, we expect that related protein translocases, including the eukaryotic 26S proteasome, use very similar mechanisms for ATP-dependent substrate unfolding and translocation.

Online Methods

Sample Preparation

Biotinylated ClpX single-chain hexamers, GFP-titin^{CM} I_{27} fusion proteins, and 3 kbp dsDNA handle for protein attached via ybbR tag/Sfp system were prepared as described previously[8]. Tethers were assembled in a buffer (25 mM HEPES-KCl [pH 7.4], 20 mM MgCl2, 100 mM KCl, and 0.5 mM EDTA) supplemented with [ATP] = 5 mM with ATP regeneration system[30]. Trace amounts of VO_4^{3-} (Sigma) [500 nM and 750 nM] were added to the buffer in presence of 5mM [ATP]. All single-molecule experiments required 500 nM of ClpP for the formation of the ClpXP complex.

Data Collection

We used a dual-trap optical trapping instrument with a 1064 nm laser in passive mode. The unfolded polypeptide contour length was calculated as previously described[8,9].

Data Analysis

Pause-free velocity was calculated as the end-to-end distance Δx/Δt, after removing pauses longer than 1-1.5s in the Δt component. Steps and dwells were analyzed using pairwise distribution and *t*-test[12]. Data were filtered to 60-100Hz for the *t*-test, and at 15-25 Hz and binned into 0.3 and 0.4 nm for the pairwise distributions. The unfolding events and its related measurements were measured by a previously described method[9].

Fraction of ATPγS bound molecules to the hexamer

We calculated the fraction of ATPγS molecules bound to the ClpX hexamer as previously reported[8]. Because ClpX has only four available nucleotide-binding sites at every cycle despite being a hexamer[14,15], we computed the probability of *i* or more ATPγS molecules binding to the motor is given by $\sum_i^n \begin{pmatrix} 4 \\ i \end{pmatrix} p^i q^{4-i}$, where *p* is the fraction of ATPγS molecules bound to ClpXP at a particular [ATPγS], and *q = 1- p*, which includes both the fraction of empty subunits and bound to a nucleotide other than ATPγS. To calculate *p* we used the values of the dissociation constants of ATP ($K_d^{(\mathrm{ATP})}$) and ATPγS ($K_d^{(\mathrm{ATP}\gamma S)}$) in a buffer containing a specific mixture of [ATP] and [ATPγS]. We used the following equation:

$$p=\frac{[\mathrm{ATP}\gamma S]K_d^{(\mathrm{ATP})}}{K_d^{(\mathrm{ATP}\gamma S)}K_d^{(\mathrm{ATP})}+[\mathrm{ATP}\gamma S]K_d^{(\mathrm{ATP})}+[\mathrm{ATP}]K_d^{(\mathrm{ATP}\gamma S)}}$$

We used the previously reported K_M values of ATP (57uM) and ATPγS (29uM) to establish an upper-bound estimate for the Kd value[8].

Measurements of ATPase rate

The ATP hydrolysis rate of wild type ClpXP and GYVG mutants was measured using an NADH-coupled ATP-regeneration system as previously described[6,8,9]. Assembled hexamers of ClpX (0.3 μM) were mixed with ClpP (1.5 μM) in a ClpX-100 buffer (25 μM HEPES pH 7.6, 20 mM MgCl2, 100 mM KCl, and 0.5 mM EDTA) containing an NADH-coupled regeneration system (3 U/mL pyruvate kinase, 3 U/mL lactate dehydrogenase, 1 mM NADH, and 7.5 mM phosphoenolpyruvate). The ATP-hydrolysis rate of ClpX was measured both in the presence and absence of 500μM titin$^{\mathrm{CM}}$-ssrA by monitoring the absorbance of NADH (340 nm) at 25° C.

Force dependence of translocation velocity of ClpXP

By fitting the force dependence of the pause-free velocity to a single-barrier Boltzmann equation[24], we obtained $F_{1/2}$, the externally applied opposing force at which the translocation velocity drops to half its maximum value (Fig. 4f). We fitted the data to the following equation:

$$v(F)=\frac{v_o(1+A)}{1+A\exp(F\delta/k_B T)}$$

where k_B is the Boltzmann constant, T is the absolute temperature, v_o is the velocity at zero load, δ is the distance to the transition state, and A is a dimensionless constant that determines the ratio of times associated with force dependent versus force-independent reaction steps. Using the data shown in Figure 4f, we obtained the following parameters for WT: $v_o = 8.7 \pm 1.6$ nm/s; $\delta = 0.96 \pm 0.4$ nm; and $A = 0.01 \pm 0.1$. The small value of A suggests that a force-independent reaction is rate limiting overall for overall ClpXP translocation. Similarly, we obtained the following parameters for YA14: $v_o = 10.7 \pm 1.4$ nm/s; $\delta = 1.41 \pm 0.7$ nm; and $A = 0.005 \pm 0.015$.

Extrapolation based on the single-barrier Boltzmann model predicts that translocation for WT would reach 5% of v_o at 32 pN, which could be accounted as the stall force of ClpXP, consistent with the previously reported stall force for ClpXP[10]. Similarly, extrapolation based on the single-barrier Boltzmann model predicts that translocation for YA14 would reach 5% of v_o at 23.5 pN, a value significant smaller compared to WT.

Calculation of Power and Work for WT and mutant ClpX

The power output (P) of ClpXP working against an opposing force is the product of the force (F_M) it applies to a substrate and translocation velocity ($v = d/t$), where d is the burst size and t is the time needed to complete a dwell/burst cycle, i.e. its dwell duration. Thus, $P = (F_M)(v) = (F_M)(d/t) = W/t$, where W is the work performed by the motor in every cycle. For WT ClpXP and its mutants, we calculated the power output at $F_{1/2}$, a condition where the product of the motor's force and velocity at this force is close to the maximum power output of the motor. For WT, we calculated $P_{WT} = F_{1/2} \cdot v(F_{1/2}) = 20.5\text{ pN} \cdot 4.4\text{ nm/s} = 90.2\text{ pN nm s}^{-1}$. For the YA14 mutant, we determined $P_{YA14} = 15.1\text{ pN} \cdot 5.3\text{ nm/s} = 80\text{ pN nm s}^{-1}$.

The stronger grip of the VF14 mutant prevented us from directly determining its $F_{1/2}$, and therefore P_{VF14}. However, based on the similar GFP unfolding probabilities for the V154F and Y153A mutants (Fig. 6b), our model suggests that $P_{VF14} \approx P_{YA14}$.

Supplementary Material

Refer to Web version on PubMed Central for supplementary material.

Acknowledgments

We thank the members of the Bustamante laboratory S. Liu, R. Gabizon, and S. Tafoya for helpful discussions. We also acknowledge M. Sen, K. Nyquist and R. Maillard for the data obtained with ATPγS. This research was supported by NIH grants R01GM071552 & R01GM032543 (C.B.: Mechanochemistry of molecular motors), NIH grant R01-GM094497 (A.M.: ATP-dependent protein degradation by AAA+ proteases), the Searle Scholars Program (A.M.), the Howard Hughes Medical Institute (C.B. and A.M.: Laboratory infrastructure and support) and the U.S. Department of Energy Office of Basic Energy Sciences Nanomachine program, under Contract No. DE-AC02-05CH11231 (C.B.: Optical tweezers development).

References

1. Moore SD, Sauer RT. Ribosome rescue: tmRNA tagging activity and capacity in Escherichia coli. Mol Microbiol. 2005; 58:456–466. [PubMed: 16194232]
2. Gottesman S, Roche E, Zhou Y, Sauer RT. The ClpXP and ClpAP proteases degrade proteins with carboxy-terminal peptide tails added by the SsrA-tagging system. Genes Dev. 1998; 12:1338–47. [PubMed: 9573050]
3. Kim YI, Burton RE, Burton BM, Sauer RT, Baker Ta. Dynamics of substrate denaturation and translocation by the ClpXP degradation machine. Mol Cell. 2000; 5:639–48. [PubMed: 10882100]
4. Baker, Ta, Sauer, RT. ClpXP, an ATP-powered unfolding and protein-degradation machine. Biochim Biophys Acta. 2012; 1823:15–28. [PubMed: 21736903]
5. Martin A, Baker Ta, Sauer RT. Diverse pore loops of the AAA+ ClpX machine mediate unassisted and adaptor-dependent recognition of ssrA-tagged substrates. Mol Cell. 2008; 29:441–50. [PubMed: 18313382]
6. Martin A, Baker Ta, Sauer RT. Pore loops of the AAA+ ClpX machine grip substrates to drive translocation and unfolding. Nat Struct Mol Biol. 2008; 15:1147–51. [PubMed: 18931677]
7. Siddiqui SM, Sauer RT, Baker Ta. Role of the processing pore of the ClpX AAA+ ATPase in the recognition and engagement of specific protein substrates. Genes Dev. 2004; 18:369–74. [PubMed: 15004005]
8. Sen M, et al. The ClpXP protease unfolds substrates using a constant rate of pulling but different gears. Cell. 2013; 155:636–46. [PubMed: 24243020]
9. Maillard, Ra, et al. ClpX(P) generates mechanical force to unfold and translocate its protein substrates. Cell. 2011; 145:459–69. [PubMed: 21529717]
10. Aubin-Tam ME, Olivares AO, Sauer RT, Baker Ta, Lang MJ. Single-molecule protein unfolding and translocation by an ATP-fueled proteolytic machine. Cell. 2011; 145:257–67. [PubMed: 21496645]
11. Chistol G, et al. High degree of coordination and division of labor among subunits in a homomeric ring ATPase. Cell. 2012; 151:1017–28. [PubMed: 23178121]
12. Moffitt JR, et al. Intersubunit coordination in a homomeric ring ATPase. Nature. 2009; 457:446–50. [PubMed: 19129763]
13. Adachi K, et al. Coupling of Rotation and Catalysis in F1-ATPase Revealed by Single-Molecule Imaging and Manipulation. Cell. 2007; 130:309–321. [PubMed: 17662945]
14. Hersch GL, Burton RE, Bolon DN, Baker Ta, Sauer RT. Asymmetric interactions of ATP with the AAA+ ClpX6 unfoldase: allosteric control of a protein machine. Cell. 2005; 121:1017–27. [PubMed: 15989952]
15. Glynn SE, Martin A, Nager AR, Baker Ta, Sauer RT. Structures of asymmetric ClpX hexamers reveal nucleotide-dependent motions in a AAA+ protein-unfolding machine. Cell. 2009; 139:744–56. [PubMed: 19914167]
16. Stinson BM, et al. Nucleotide Binding and Conformational Switching in the Hexameric Ring of a AAA+ Machine. Cell. 2013; 153:628–639. [PubMed: 23622246]
17. Baird CL, Harkins TT, Morris SK, Lindsley JE. Topoisomerase II drives DNA transport by hydrolyzing one ATP. Proc Natl Acad Sci U S A. 1999; 96:13685–13690. [PubMed: 10570133]
18. Sharma S, Davidson aL. Vanadate-induced trapping of nucleotides by purified maltose transport complex requires ATP hydrolysis. J Bacteriol. 2000; 182:6570–6576. [PubMed: 11073897]

19. Chemla YR, et al. Mechanism of force generation of a viral DNA packaging motor. Cell. 2005; 122:683–92. [PubMed: 16143101]
20. Schnitzer MJ, Block SM. Kinesin hydrolyses one ATP per 8-nm step. Nature. 1997; 388:386–90. [PubMed: 9237757]
21. Martin A, Baker Ta, Sauer RT. Protein unfolding by a AAA+ protease is dependent on ATP-hydrolysis rates and substrate energy landscapes. Nat Struct Mol Biol. 2008; 15:139–45. [PubMed: 18223658]
22. Martin A, Baker Ta, Sauer RT. Rebuilt AAA + motors reveal operating principles for ATP-fuelled machines. Nature. 2005; 437:1115–20. [PubMed: 16237435]
23. Iosefson O, Nager AR, Baker Ta, Sauer RT. Coordinated gripping of substrate by subunits of a AAA+ proteolytic machine. Nat Chem Biol. 2015; 11:201–6. [PubMed: 25599533]
24. Wang MD, et al. Force and velocity measured for single molecules of RNA polymerase. Science. 1998; 282:902–7. [PubMed: 9794753]
25. Glynn SE, Nager AR, Baker Ta, Sauer RT. Dynamic and static components power unfolding in topologically closed rings of a AAA+ proteolytic machine. Nat Struct Mol Biol. 2012; 19:616–22. [PubMed: 22562135]
26. Keller D, Bustamante C. The mechanochemistry of molecular motors. Biophys J. 2000; 78:541–56. [PubMed: 10653770]
27. Visscher K, Schnitzer MJ, Block SM. Single kinesin molecules studied with a molecular force clamp. Nature. 1999; 400:184–9. [PubMed: 10408448]
28. Olivares AO, Nager AR, Iosefson O, Sauer RT, Baker Ta. Mechanochemical basis of protein degradation by a double-ring AAA+ machine. Nat Struct Mol Biol. 2014; :1–6. DOI: 10.1038/nsmb.2885 [PubMed: 24389540]
29. Iosefson O, Olivares AO, Baker TA, Sauer RT. Dissection of axial-pore loop function during unfolding and translocation by a AAA+ proteolytic machine. Cell Reports. 2015; 12:1032–41. [PubMed: 26235618]
30. Kenniston JA, Baker Ta, Fernandez JM, Sauer RT. Linkage between ATP consumption and mechanical unfolding during the protein processing reactions of an AAA+ degradation machine. Cell. 2003; 114:511–20. [PubMed: 12941278]

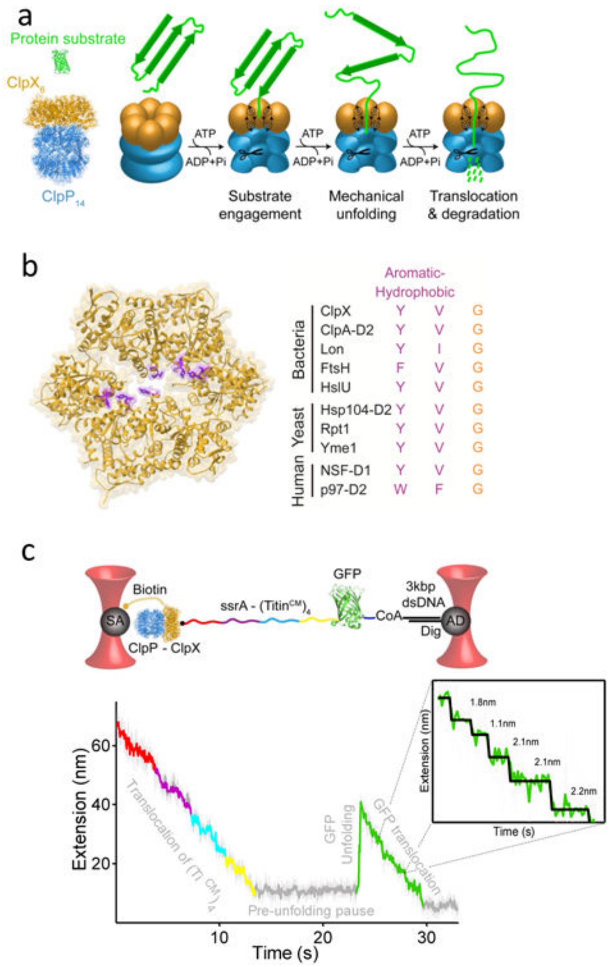
a
Protein substrate
ClpX$_6$
ClpP$_{14}$
ATP
ADP+Pi
ATP
ADP+Pi
ATP
ADP+Pi
Substrate engagement
Mechanical unfolding
Translocation & degradation
b
Aromatic-Hydrophobic
Bacteria
ClpX Y V G
ClpA-D2 Y V G
Lon Y I G
FtsH F V G
HslU Y V G
Yeast
Hsp104-D2 Y V G
Rpt1 Y V G
Yme1 Y V G
Human
NSF-D1 Y V G
p97-D2 W F G
c
Biotin
SA
ClpP - ClpX
ssrA - (Titin^{CM})$_4$
GFP
CoA
3kbp dsDNA
Dig
AD
Extension (nm)
60
40
20
Translocation of (Ti^{CM})$_4$
Pre-unfolding pause
GFP Unfolding
GFP translocation
10
20
30
Time (s)
Extension (nm)
1.8nm
1.1nm
2.1nm
2.1nm
2.2nm
Time (s)

Figure 1. Single-molecule Trajectories of Protein Unfolding and Translocation by ClpXP

(a) Side view of the ClpXP structural model (*left*) and cartoon of the general mechanism of protein degradation by ClpXP (*right*) (ClpX PDB ID: 3HWS; ClpP PDB ID: 3MT6).

(b) *Left:* Top view of the ClpX hexameric ring showing the translocating GYVG loops (pore-1 loops) in purple (PDB ID: 3HWS[15]). *Right*: Aromatic-hydrophobic motif in the translocating pore-1 loops of prokaryotic and eukaryotic AAA+ protein translocases.

(c) *Top*: Experimental geometry of the dual-trap optical tweezers assays. ClpXP is immobilized on a micron-sized bead coated with streptavidin (SA), and the substrate is bound to an anti-digoxigenin-coated bead (AD) via a DNA handle. The ssrA-tagged substrate has four permanently unfolded (carboxymethylated, CM) titin I27 domains (Ti^{CM}) C-terminally fused to a green fluorescent protein (GFP). *Bottom:* Single-molecule trajectory in passive mode of substrate translocation and unfolding by ClpXP. Raw data (2.5 kHz in gray) were filtered and decimated to 100 Hz (in red, purple, cyan, yellow, and green to indicate individual domains of the substrate). *Inset*: Segment of a ClpXP translocation region displaying individual translocating bursts. Raw data were filtered and decimated to 800 Hz (in gray) or 70 Hz (in green). *t* test fits to the data are shown in black.

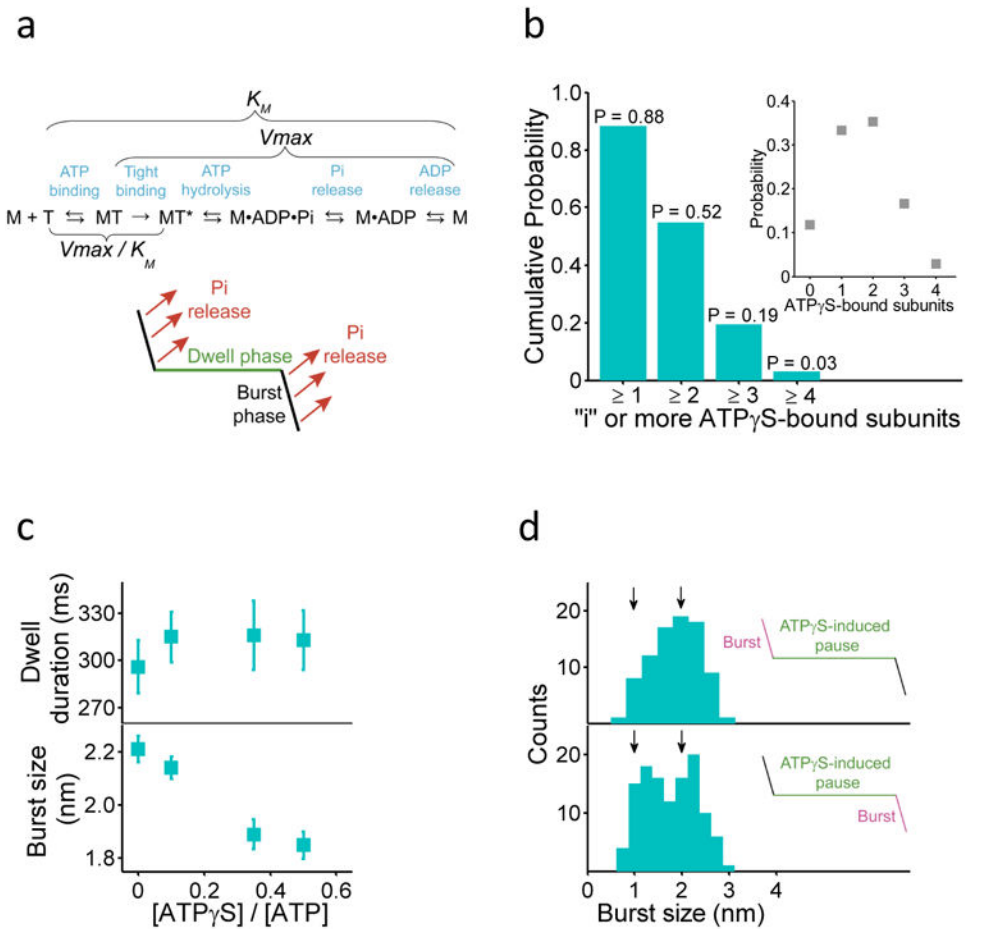

Figure 2. Location of ATP hydrolysis in the Dwell-Burst Cycle

(a) *Top:* General scheme of the ATPase cycle in a single ClpX subunit "motor" (M). The subunit binds ATP (T), undergoes a tight-binding transition, hydrolyzes ATP, and finally releases Pi and ADP. The Michaelis constant (K_M), the effective catalytic rate constant (*Vmax*), and the effective binding rate constant (*Vmax/*K_M) depend on specific rate constants of the ATPase cycle, as indicated by the brackets. *Bottom*: ClpXP translocation is composed of two phases: dwell and burst. Pi release coincides with the power stroke of the motor[8].

(b) Cumulative probability of "*i*" or more ATPγS molecules bound to the motor at [ATP] = 500 μM and [ATPγS] = 200 μM. *Inset:* Individual probability for certain numbers of ATPγS molecules bound to the motor under the same buffer condition. See Online methods for calculation details.

(c) Dependence of the dwell duration and burst size on [ATPγS] (mean ± SEM). *n* = 1060 dwells and 1154 bursts).

(d) Size distribution of the bursts that precede *(Top, n* = 98 bursts) or follow *(Bottom, n* = 118 bursts) an ATPγS-induced pause.

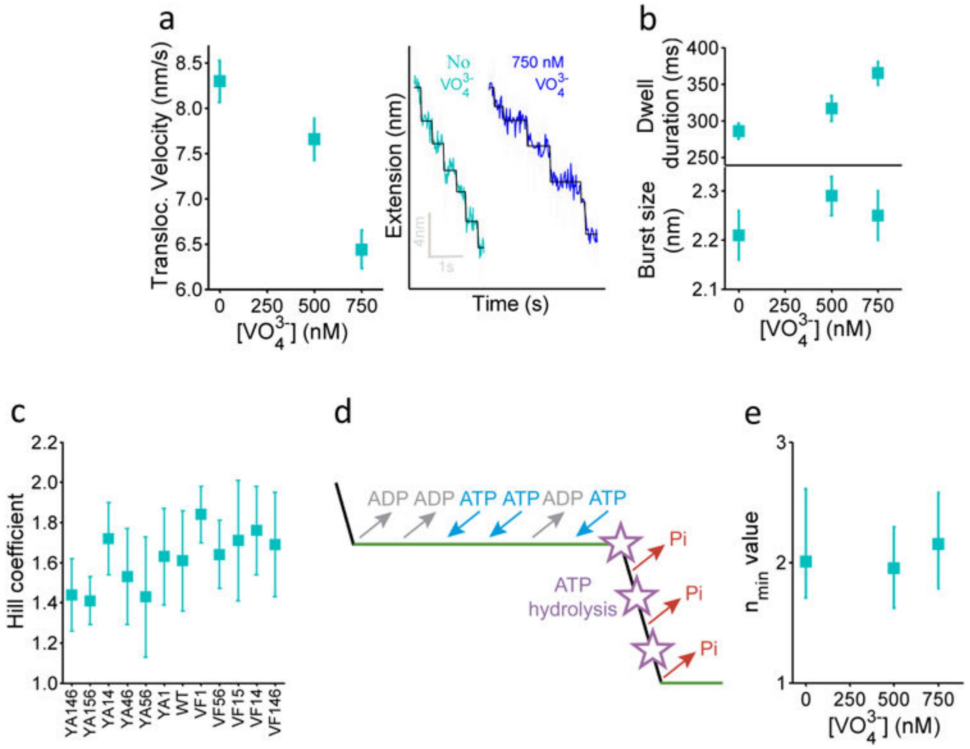

Figure 3. Localization of ADP Release within the Dwell-Burst Cycle

(a) *Left:* Dependence of translocation velocity on [VO_4^{3-}] (mean ± SEM) at [ATP] = 5 mM. *Right:* Representative trajectories of ClpXP translocation in the absence and presence of VO_4^{3-}. Raw data were filtered and decimated to 800 Hz (in gray) or 70 Hz (in green and blue). *t* test fits to the data are shown in black.

(b) Dependence of the dwell duration and burst size on [VO_4^{3-}] (mean ± SEM). The mean dwell duration in the absence and presence of 750 nM VO_4^{3-} was determined to be different with p = 1.04e-5 (two-sample Kolmogorov-Smirnov test, null hypothesis: both distributions identical). *n* = 927 dwells and 856 bursts.

(c) Hill coefficient of WT ClpXP and GYVG pore-loop mutants. Hill coefficients were obtained from bulk ATPase measurements in the presence of 1500 μM Ti$^{\mathrm{CM}}$-ssrA substrate. Error bars represent 95 % confidence intervals estimated by fitting the data to the Hill equation.

(d) Diagram of the location of each chemical transition of the ATPase cycle during the dwell/burst cycle of the motor.

(e) Dependence of the $\mathrm{n}_{\mathrm{min}}$ value on [VO_4^{3-}]. Error bars represent 95 % confidence intervals estimated via bootstrapping.

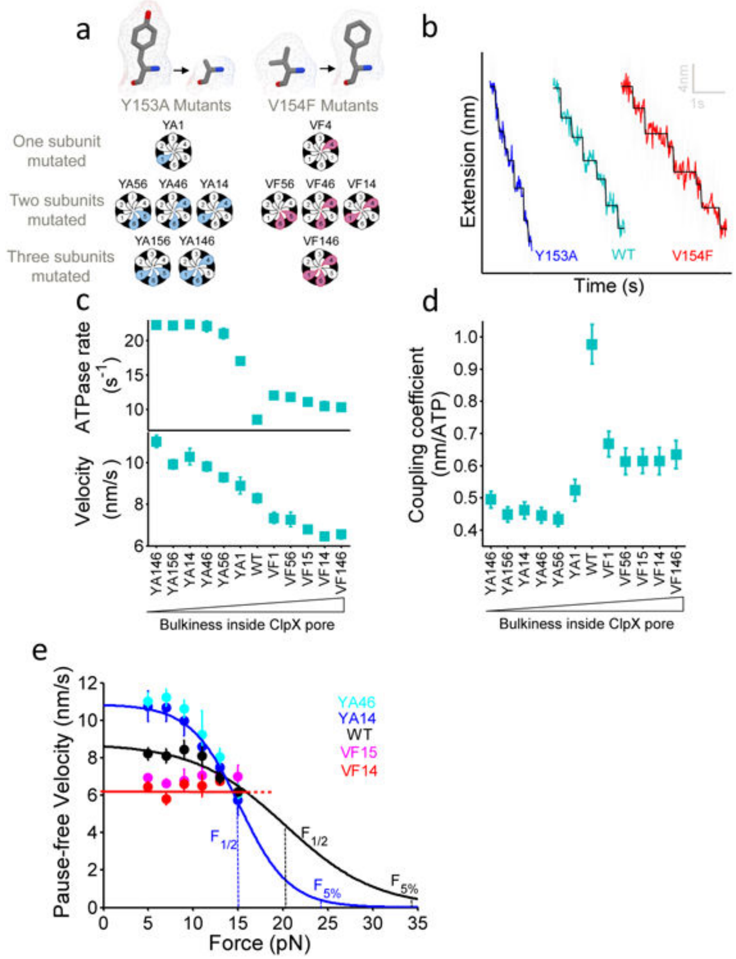

Figure 4. Effects of GYVG Mutations on the Mechanochemical Coupling of ClpXP

(a) The GYVG pore-loop mutations Y153A or V154F were introduced in one, two, or three subunits in different geometries. Numbers behind YA and VF indicate which subunits in the single-chain ClpX hexamer were mutated.

(b) Representative single-molecule trajectories for translocation by WT ClpXP and GYVG mutants. Raw data were filtered and decimated to 800 Hz (in gray) or 60 Hz (in blue, green, and red). *t* test fits to the data are shown in black.

(c) *Top:* ATPase rates of WT ClpXP and GYVG mutants during protein translocation, i.e. in the presence of saturating Ti^{CM}-ssrA substrate (500 μM). Rates have an error of approximately ± 5% based on three independent measurements. Numbers indicate mutated subunits in the ClpX hexamer. The X axis presents a series of mutants with the bulkiness inside the ClpX pore increasing from left to right. *Bottom*: Pause-free translocation velocities of GYVG mutants (mean ± SEM) at [ATP] = 5 mM.

(d) Coupling coefficient (ε) between substrate translocation and ATP consumption for WT ClpXP and GYVG mutants (mean ± SEM) at [ATP] = 5 mM.

(e) Force-dependence of translocation velocity for WT ClpX and GYVG mutants (mean ± SEM) at [ATP] = 5 mM. The solid line shows a fit to a single-barrier Boltzmann equation[24]. $F_{1/2}$ refers to the force at which the motor has half its maximum velocity, while $F_{5\%}$ indicates to the force at which the motor reaches 5% of its maximum velocity.

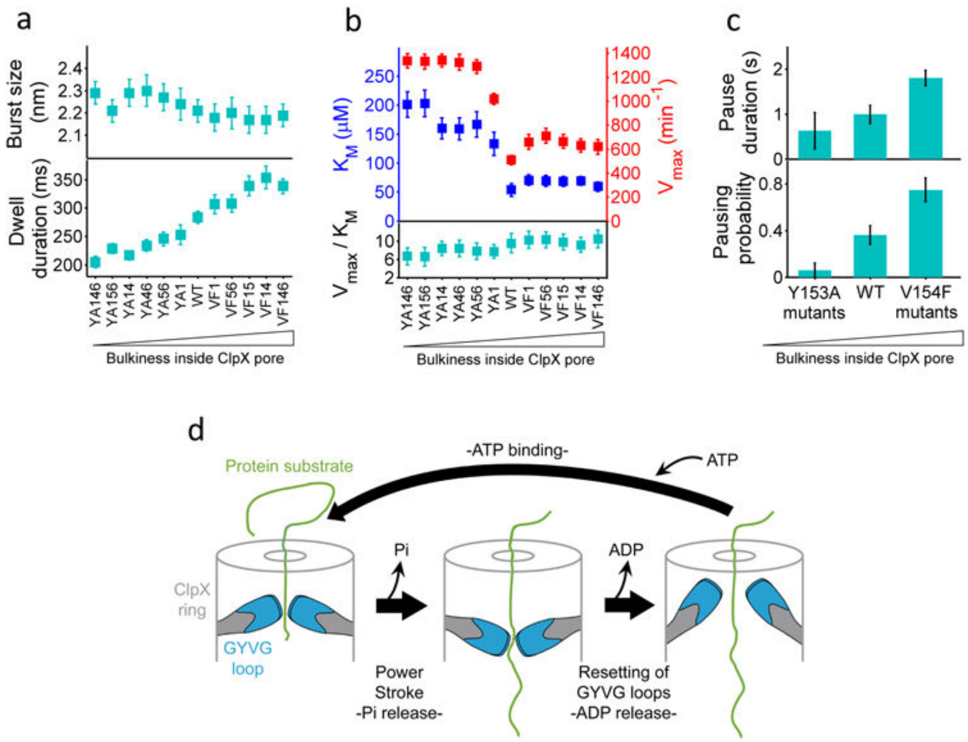

Figure 5. Effects of GYVG Mutations on the Dwell-Burst Cycle of ClpXP

(a) Burst size and dwell duration for WT ClpXP and its GYVG mutants (mean ± SEM) at [ATP] = 5 mM. The X axis presents a series of mutants with the bulkiness inside the ClpX pore increasing from left to right. Numbers indicate positions of mutated subunits in the ClpX hexamer. In average, 200 dwells and 150 bursts were analyzed for each GYVG mutant.

(b) Values of Vmax and Vmax/K_M for ATP hydrolysis by WT ClpXP and its GYVG mutants (mean ± SEM). K_M and Vmax values were determined by Michaelis-Menten analyses ($n = 3$ independent experiments).

(c) Effect of GYVG mutations on the duration and frequency of the sequence-induced pause originating from the bulkiest region of the GFP protein substrate (Supplemental Fig. 6). The pausing probability for this specific region was calculated as the number of traces showing a residence time longer than 0.5 s, which corresponds to the mean residence time plus two standard deviations, divided by the total number of traces measured under those conditions: $n_{WT} = 37$ traces; $n_{VF} = 28$ traces; $n_{YA} = 42$ traces. Error bars indicate counting error.

(d) Model for the mechanochemical coupling of ClpX, where the GYVG-loop resetting occurs after the power stroke and is coupled to ADP release during the dwell phase.

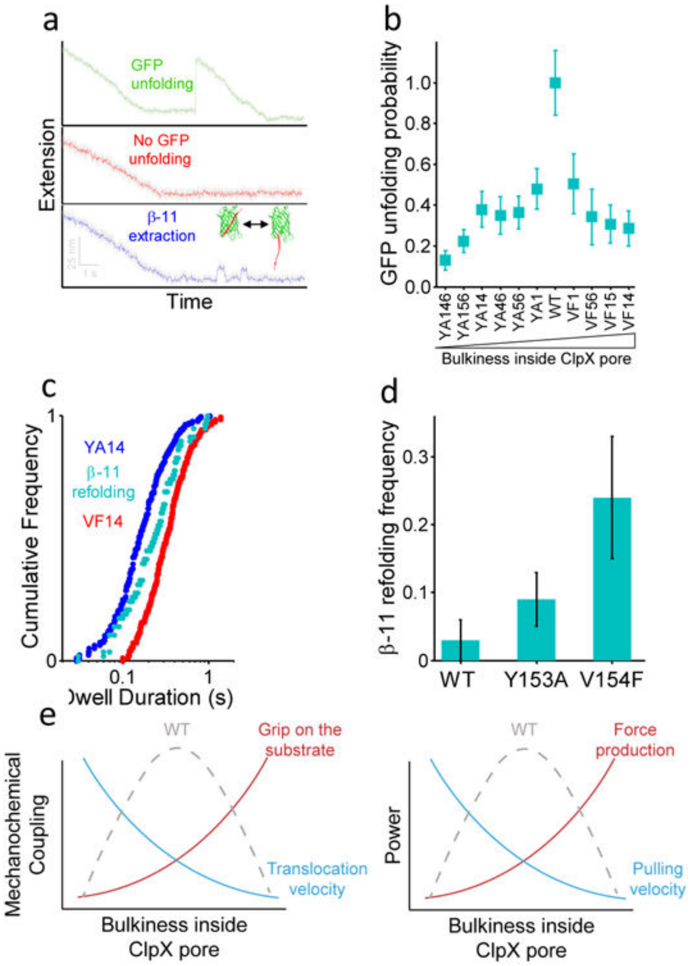

Figure 6. Effects of GYVG Mutations on the GFP unfolding efficiency of ClpXP

(a) Representative single-molecule traces that show successful GFP unfolding (*Top*), no GFP unfolding (*Middle*), and β11-strand extraction/refolding events (*Bottom*).

(b) GFP unfolding probability for WT ClpXP and its GYVG mutants at [ATP] = 5 mM. Error bars indicate counting error.

(c) Distribution of the β11-strand refolding time (cyan) versus the distribution of the dwell duration for YA14 (blue) and VF14 (red) mutants (n = 58 β11-strand refolding events).

(d) Frequency of β-11 extraction/refolding events for WT ClpXP and GYVG mutants, which was calculated as the ratio of the number of traces displaying these events divided by the total number of traces. Error bars indicate counting error.

(e) Dependence of the mechanochemical coupling and the power produced by the motor on the bulkiness inside the crowded ClpX pore. The coupling efficiency (fraction of ATP-hydrolysis cycles that result in successful translocation against an opposing force) depends on the translocation rate and the grip, i.e. the strength of interactions with the substrate. The motor power is a physical parameter that depends on the amount of work produced per unit time. Power was calculated by multiplying $F_{1/2}$ and the corresponding velocity at that force for each ClpX variant. Based on our results, both the mechanochemical coupling and the power of the ClpX motor seem to reach a maximum for the WT GYVG-loop sequence, suggesting that evolution has selected the bulkiness of the loop residues to maximize these two properties of the motor.